Modeling Sea Surface Height in the Gulf of Mexico

by

Adam C. Rigel

Submitted to the Department of Earth, Atmospheric and Planetary Sciences

in Partial Fulfillment of the Requirements for the Degree of

Bachelor of Science in Earth, Atmospheric and Planetary Sciences

at the Massachusetts Institute of Technology

May 9, 2008 [June 2008]

Copyright 2004 Adam C. Rigel All rights reserved.

The author hereby grants to M.I.T. permission to reproduce and distribute publicly paper and electronic copies of this thesis and to grant others the right to do so.

Author_____ Signature redacted _____

Department of Earth, Atmospheric and Planetary Sciences
May 17, 2004

Certified by___ Signature redacted _____

Kerry Emanuel
Thesis Supervisor

Accepted by___ Signature redacted _____

Samuel Bowring
Chair, Committee on Undergraduate Program

MASSACHUSETTS INSTITUTE OF TECHNOLOGY
OCT 24 2017
LIBRARIES
ARCHIVES

The author hereby grants to MIT permission to reproduce and to distribute publicly paper and electronic copies of this thesis document in whole or in part in any medium now known or hereafter created.

Abstract

A model was created to form synthetic plots of sea surface height (SSH) from monthly SSH statistics in the Gulf of Mexico generated from satellite laser altimetry data. SSH is a signal of the upper ocean mixed layer heat content and is an input for hurricane intensity models. A significant ocean feature in the Gulf of Mexico is the Loop Current (LC) which sheds warm eddies into the Gulf of Mexico at irregular intervals, which adds to the variability in monthly SSH readings beyond seasonal change. Satellite laser altimetry data was used from October 14th 1992 to May 23rd 2007. The SSH data included an area of the Gulf of Mexico (16°N-30°N latitude, 80°W-100°W longitude) with a resolution of 1/3° by 1/3° on a Mercator grid. Monthly SSH averages, variances, and covariances were created from a total of 763 samples, which allowed for approximately 65 samples per month. Once monthly SSH averages, variances, and covariances were made, synthetic plots were made by using a Karhunen-Loève transform, the Singular Variable Decomposition of the SSH monthly covariance, and random vector composed of random numbers in a Gaussian distribution. Differences in synthetic SSH plots compared to individual SSH observations could vary greatly; the average of all synthetic SSH plot nodes differed by no more than plus or minus 10 cm. The difference between observed and synthetic SSH variance was no more than 400 cm^2. The large differences occurred in the in the eddy shedding region of the LC. To assess the effectiveness of the model, the synthetic SSH model will need to be used in a hurricane intensity model.

1. Introduction

Over the past several decades, hurricane tracking and modeling have become more sophisticated, but these models must still be improved because of the economic implications of a destructive storm. In the recent past, several large storms have hit communities on the Gulf of Mexico, causing billions of dollars in damage. The storms in the 2004 hurricane season caused $24 billion in damage to Gulf Coast communities (USA Today, 2005). In 2005, Hurricane Katrina showed how costly a hurricane can be causing an estimated $125 billion in damage (Emanuel, 2006) of which $40-$60 billion (Risk Management Solutions, 2005) of that damaged was insured loss. Given the destructive power

of these storms, as people continue to occupy the Gulf Coast region, it is especially important for insurers to understand the risk associated with insuring homes and businesses in the region. Without a good knowledge of risk, insurers cannot develop proper capital reserves and re-insurance plans, thus risking bankruptcy from major events. Also, there is a cost associated with evacuations. If models cannot properly predict intensity or there is simply too much uncertainty, then a weaker-than-predicted storm can lead to unnecessary evacuation and thus loss of time and convenience for many residents, unnecessary costs to government entities, and loss of economic activity (Emanuel, 1999).

Understanding the development of intense hurricanes will help in developing hurricane intensity models and thus help to assess risk not only in the Gulf Coast Region, but also in other coastal regions throughout the world. One important input for developing hurricane intensity models is the interaction of hurricanes with ocean eddies (Lin, 2005).

The interaction of ocean eddies and hurricanes have been observed to greatly increase hurricane intensity in a short time frame (Lin, 2005). When they passed over warm water eddies or other warm water features, Hurricanes in the Atlantic, such as Hurricanes Opal, Mitch, and Bret rapidly intensified from Saffir-Simpson category 1 to category 4 within 24-36 hours (Lin, 2005). Although ocean features are not the sole factor in rapid intensification, their role in rapid intensification of hurricanes in the Gulf of Mexico can pose a great threat to Gulf Coast communities (Lin, 2005). Also, passage over cold eddies should lead to potentially rapid weakening of the storms.

2. Relationship of Ocean Features and Hurricane Intensity

As seen with Hurricanes Opal, Mitch, and Bret, ocean features have the potential to rapidly intensify a hurricane. Heat from these features is a driving force to create and intensify storms. A tropical cyclone may be described as a heat engine in which the heat source is evaporation from the sea surface and the efficiency is proportional to the difference between the sea surface temperature and the much lower temperature at the top of the storm (Emanuel, 2003). Given that hurricanes develop in warm tropical seas whose sea surface temperature (SST) is greater than 26 degrees Celsius (Emanuel, 2003), warm tropical seas, like the Gulf of Mexico, are areas of great storm producing potential. Should an anomalous ocean feature, such as a warm eddy, occur in the path of a storm, the heat engine cycle can become more efficient and intensify the storm.

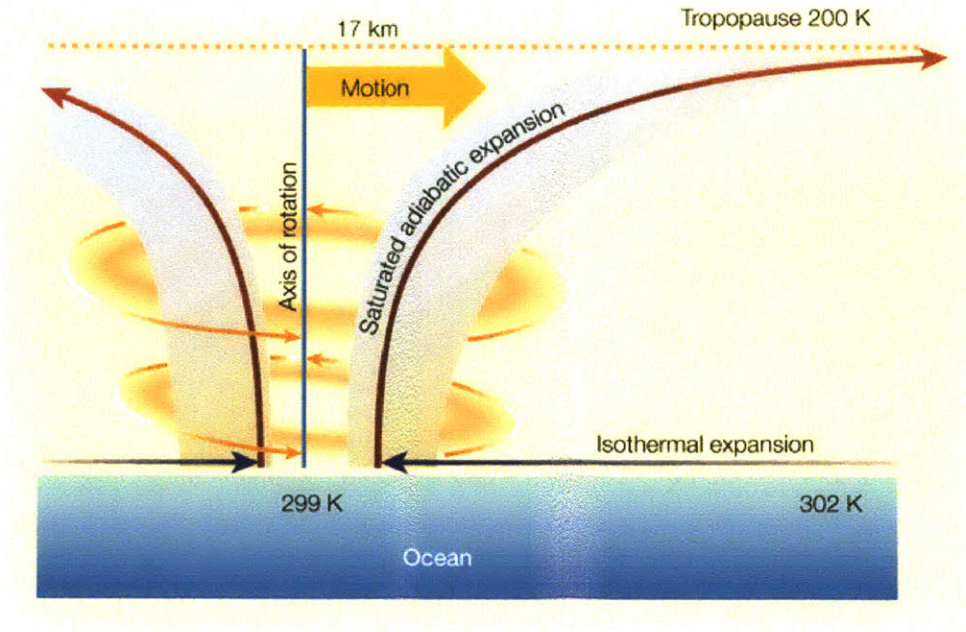

Figure 1. Schematic of hurricane formation. Hurricane formation is similar to a heat engine where efficiency is proportional to the difference in SST and the top of the storm.

Important for the increase in hurricane intensity is not just SST, but also the depth of the mixed layer in the upper ocean. Hurricanes will alter the temperature profile of the upper ocean as seen by the decrease in ocean surface temperatures after the passing of a hurricane, where SST falls up to 5 degrees Celsius in the wake of the storm (Cione, 2003). Cooling SST is a result of turbulent mixing of the upper ocean (Emanuel, 2003).

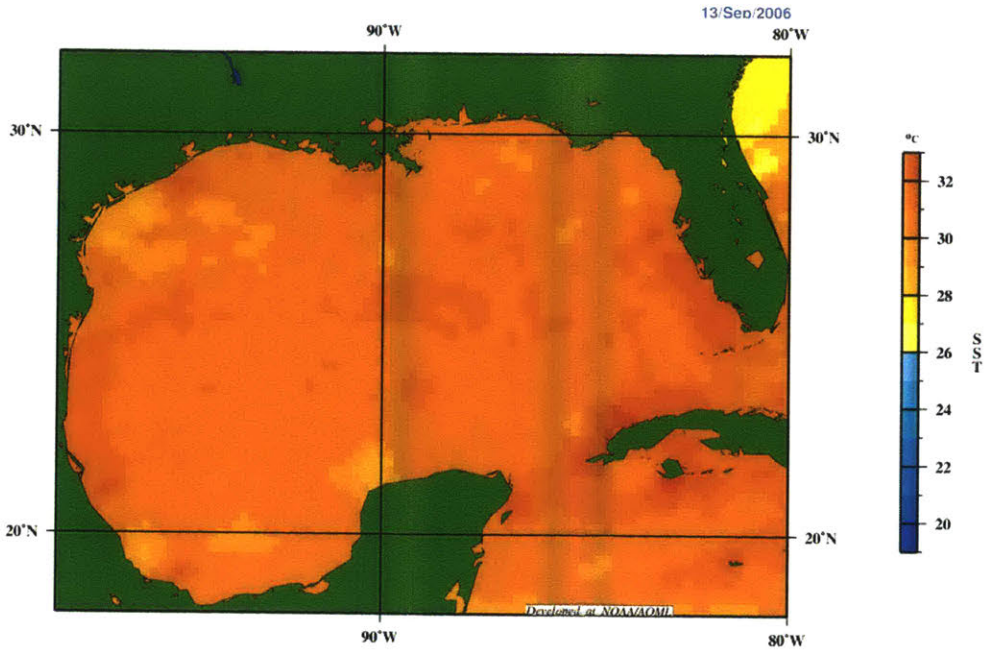

Figure 2. September Sea Surface Temperatures (SST) in the Gulf of Mexico. SST in the Gulf of Mexico during peak hurricane season is greater than the hurricane formation threshhold temperature of 26 degrees Celsius. From NOAA.

Therefore, It is also important for hurricane development that the upper layer of the ocean be well mixed to sufficient depth, rather than have just warm surface temperatures with a sharp decline at depth (Leipper, 1972). As the storm cools the surface waters, they become denser and sink to create a convective layer in the upper ocean and the storm will continue to deepen this layer by turbulent mixing (Emanuel, 2003). Unless this layer is deep, there will be little heat content in the upper ocean to keep SST high enough to power convection in the hurricane and promote the development of the storm and an increase in storm intensity (Leipper, 1972).

One of the significant warm water features in the Gulf of Mexico that increases the size of the upper ocean mixed layer and heat reservoir is the Loop Current (LC) (Zavala-Hidalgo, 2005).

3. Gulf of Mexico Upper Ocean Features - The Loop Current

A significant warm water feature in the Gulf of Mexico which can increase the amount of heat content in the upper mixed layer which can greatly intensify hurricanes is the Loop Current (LC).

The LC is a warm water current that is a main feeding branch of the Gulf Stream (Zavala-Hidalgo, 2005). The current runs from the Yucatan Peninsula through to the Florida Channel where it merges with the Gulf Stream. However, the path through these two regions varies through time. The LC may have a nearly straight path between those two points, but this path will evolve such that the LC from the Yucatan rushes northward into the Gulf and follows an anticyclonic path as it turns back to the South and exits through the Straits of Florida. Once the current reaches a critical, horseshoe-like shape, it becomes unstable and sheds an anticyclonic eddy of warm water (Hurlbut, 1980). Once this eddy forms, it may circulate within the meander of the LC, so the eddy may take several days to shed from the LC (Zavala-Hidalgo, 2005). The evolution of the LC can be seen in figure 3.

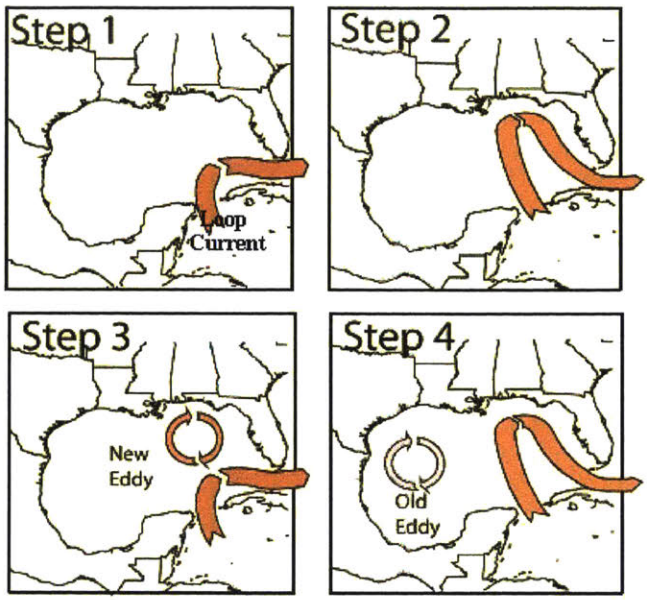

Figure 3. Loop Current Progression. The LC bends northward into the Gulf of Mexico where it sheds an eddy. The LC returns to its original path while the eddy travels westward and the cycle starts again. From NOAA.

The shed eddy has a diameter of around 250km and a depth of 800m. This eddy moves westward at an average speed of 2.4 cm/s and dissipates far from the LC (Hurlbut, 1980). Several of these eddies can exist within the Gulf as they continue to decay with time (Oey, 2003). As the eddies diminish , their heating potential decreases, but still provides an enhanced heat reservoir as they travel westward and so can provide an area for potential rapid intensification.

However, eddies are not shed in regular intervals and present a problem for hurricane intensity models. The frequency of eddy shedding is anywhere from 3 to 17 months (Oey, 2003). This irregularity can introduce errors in the hurricane intensity model since they provide an influx of warm water in the Western Gulf and thus variability in the depth of the mixed layer and size of the

heat reservoir. However, the variability that the eddy intrusions provide is not well documented, so intensity models must rely on seasonal mean upper-ocean thermal structure such as from Levitus (1982).

Given that the Loop Current (LC) can deepen the mixed layer by introducing warm water eddies (Hurlbut, 1980), in order to relate the LC and eddies to hurricane intensity modeling, we must understand how the LC adds to the variability of the mixed layer in the Gulf of Mexico.

4. Measurement of Upper Ocean Features - Sea Surface Height

One measurement that can be used to deduce the location of warm water features such as eddies is the measurement of sea surface height (SSH) relative to the geoid of the Earth. Changes in SSH can indicate changes in the thermal and salinity structure (Willis, 2004) as well as ocean floor topography from changes in gravity (Smith, 2001). However, the dominant factor in causing seasonal changes in SSH is oceanic heat content and temperature (Willis, 2004). The change in upper ocean heat content causes an expansion of the water column and thermosteric sea level rise. Since the bulk of change in ocean heat content occurs in the upper ocean, SSH can show us changes in upper level oceanic heat content and deepening of the mixed layer (Willis, 2004), which, as discussed earlier, is a factor important for the development of hurricane intensity. Since an increase in SSH shows an area of higher oceanic heat content, SSH altimetry can be used to find warm water features such as the LC.

In order to measure the location and depth of the LC and its shed eddies, two measurement networks were developed: Argo floats and satellite laser altimetry missions, such as Poseidon/TOPEX. The Argo network is comprised of 3000 floats deployed around the world, providing measurements of salinity and temperature at various depths of the water column up to 2000m (Roemmich, 2000). The Argo network also works in tandem with the Poseidon/TOPEX, which provides measurements of average SSH and ocean surface topography using laser altimetry. By using changes in SSH, one can infer aspects of the subsurface water column such as its temperature structure (Fu, 1994). TOPEX/Poseidon was one of the first satellite missions to map SSH around the globe, but several other missions were carried out over the last decade to map SSH, including Jason-1, Envisat, GFO, ERS-1 & 2, and Geosat. Using a combination of datasets from these missions will allow us to estimate variability in the depth of the mixed layer.

5. Intensity Model

The hurricane intensity model that will be used to incorporate SSH variability in the Gulf of Mexico is the one described by Emanuel et al. (2006). Synthetic hurricanes are developed as a function of spatial probability based on historical hurricane data. Once an origin is determined, hurricanes move based on a weighted average of ambient flow at 850 mb and 250 mb, which varies randomly with time, but is constrained to have the correct monthly means and

covariances. A constant drift correction is also applied. These factors set the path of the synthetic storm.

A deterministic numerical simulation is used along the storm's path to determine wind intensity, which depends on both atmospheric and oceanic conditions. Emanuel et al. (2004) describes this technique in more detail.

In order for this model to predict wind intensity, it must be initialized with estimates of potential intensity, upper-ocean thermal structure and wind shear along the storm's path. In particular, we will be looking at how variability of the upper-ocean thermal structure can have a significant influence on hurricane intensity.

The measure that will be used to examine and estimate upper ocean thermal structure is SSH. Based on historical observed monthly average Gulf of Mexico SSH data, synthetic SSH data will be generated. This synthetic SSH data will aid in providing an input for upper ocean thermal structure in the hurricane intensity model.

6. Sea Surface Height Dataset

. In order to create synthetic SSH data, we obtained observations of SSH. Our acquired observed SSH data is a composite of several satellite altimetry missions from Ssalto/Duacs, an AVISO-distributed product. This multi-mission data processing system contains data produced from several satellites, including Jason-1, TOPEX/Poseidon, Envisat, GFO, ERS-1 & 2, and Geosat. The

combination of data from these missions allows for more homogeneous results by reducing differences between altimetry in separate missions. All SSH readings were taken relative to the mean SSH for the 7-year period from 1993-1999.

The Ssalto/Duacs data have resolution of 1/3° latitude by 1/3° longitude on a Mercator grid, which places it within the diameter of a typical hurricane eye wall (Marks, 1985). The area of the Gulf of Mexico Ssalto/Duacs data we sampled was from 16°N-30°N latitude, 80°W-100°W longitude. The total number of grid nodes was 2684; these were placed on a 44 by 61 grid node matrix. A single SSH measurement is located at each grid node.

Ssalto/Duacs observation data span from October 14th 1992 to May 23rd 2007. Each observation time step was approximately 7 days, providing over 60 SSH observations for each month over the 15 year period for an overall total of 763 individual observations for the Gulf of Mexico region.

7. Sea Surface Height Data Processing

Our goal was to be able to create synthetic SSH maps for the Gulf of Mexico within the bounds of the variability of the average SSH for each month. In order to create the synthetic SSH grid-node matricies to deduce the SSH variability for each month, each individual sample observation within the collection of observations for a month of the year was converted from a grid node matrix to a row vector. Each row vector was then strung into a column vector

containing all of the observed sample row vectors to create a matrix of all observed samples for a particular month. Using all of the observed samples, the mean SSH for each node of the row vector was computed to produce a vector for the monthly mean SSH. To compute this, all observations were added within a node and divided by the number of observations for that particular node.

Once the monthly mean SSH was computed and the observed sample matrix was created, the spatial covariance of SSH within our observed samples was determined. This process produced a covariance matrix in which the row and column lengths were equal to the number of grid nodes within each observed sample, yielding 2684 by 2684 grid nodes. From the diagonal of this covariance matrix, a variance vector for the particular month was built, which was then converted to a 44 by 61 grid node matrix to produce the variance matrix.

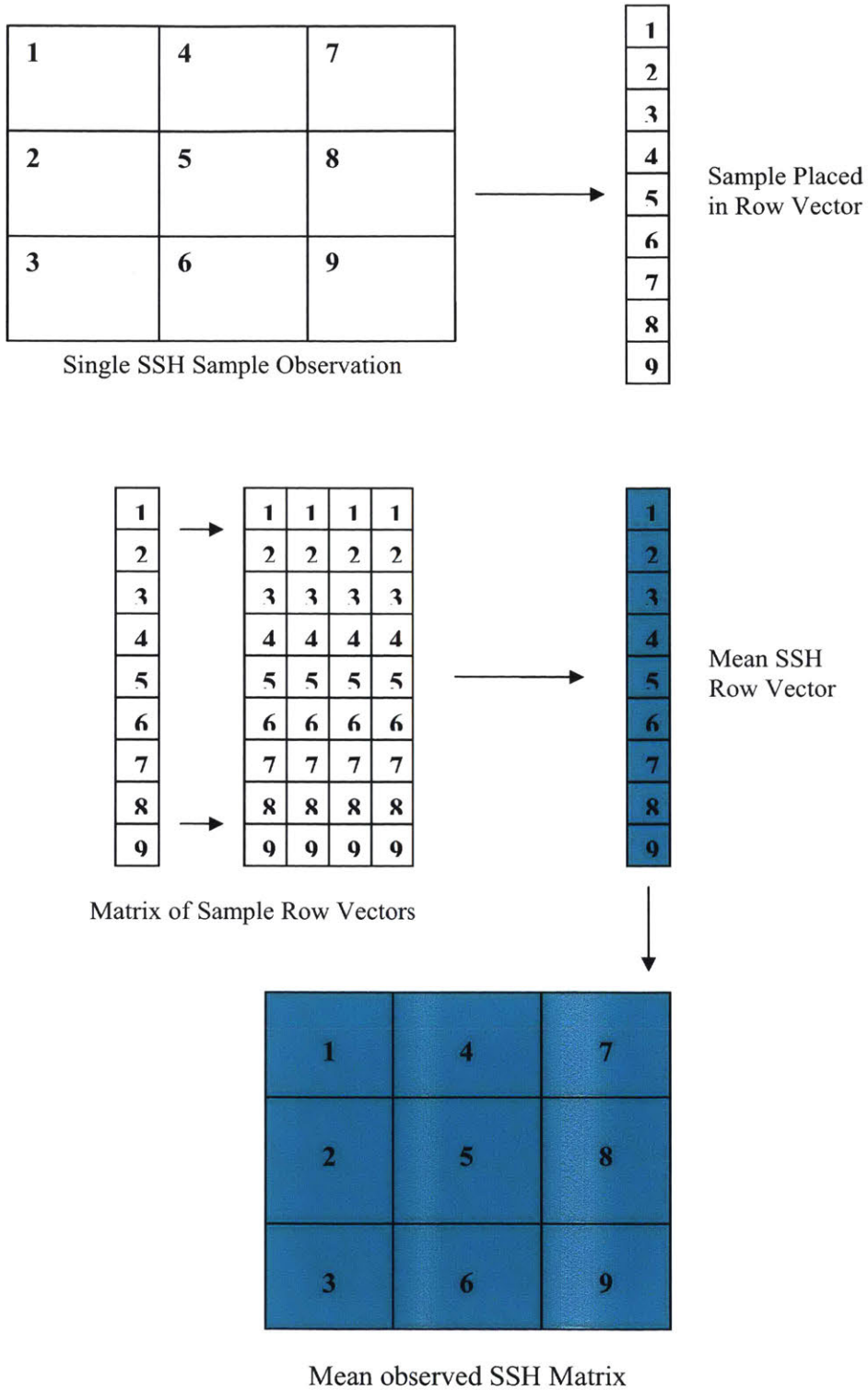

Figure 4. Schematic of the calculation observed mean monthly SSH. Individual observations were converted into row vectors. These row vectors were strung into a matrix of multiple observations for the month. The observed mean monthly SSH row vector was then produced by taking the average for all grid nodes. Lastly, the row vector was converted back to a matrix.

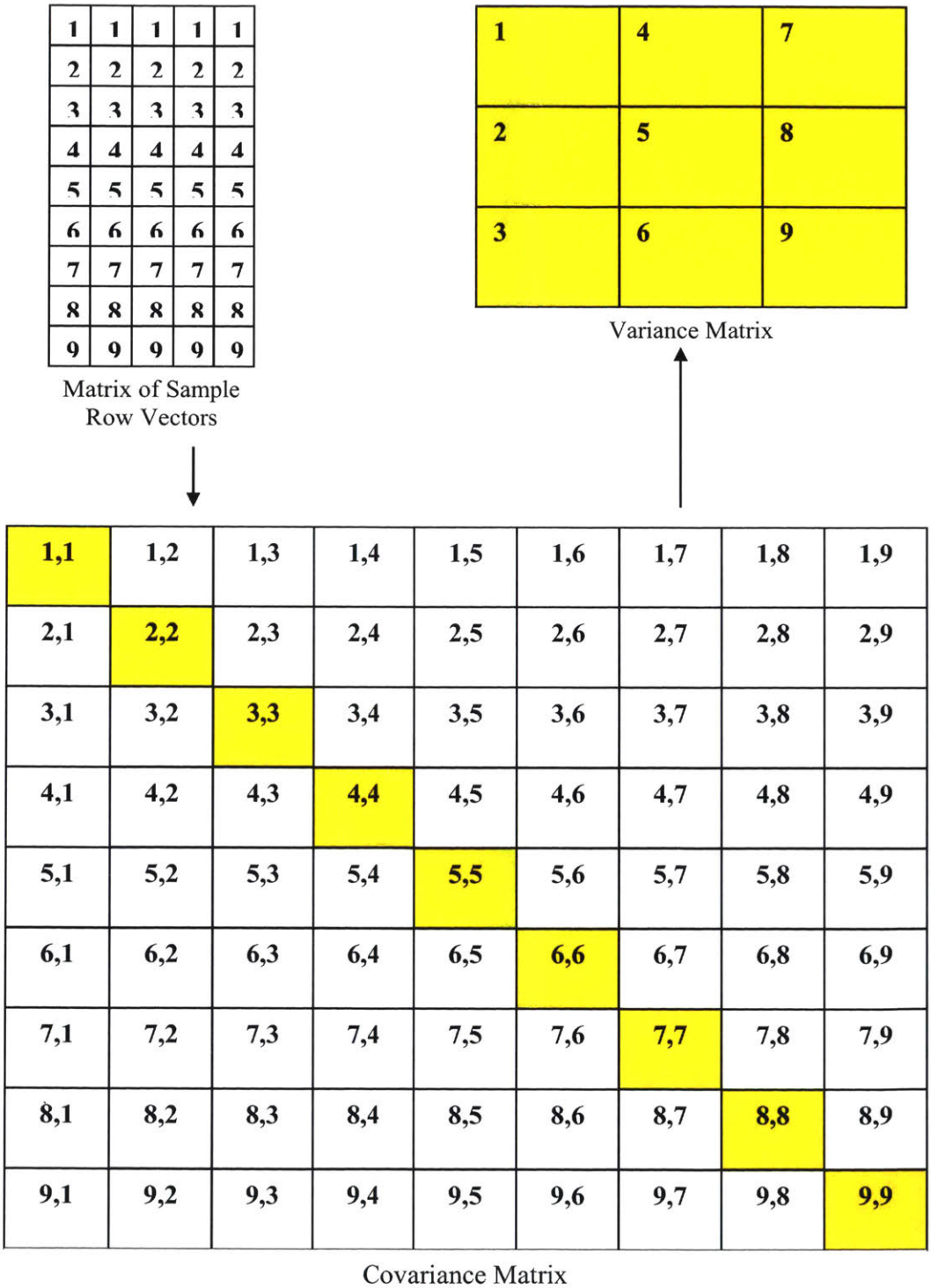

Figure 5. Observed Monthly Variance Calculation Schematic. Once multiple observations have been strung into a matrix, the covariance matrix is calculated. The variance matrix simply is derived from the diagonal of the covariance matrix.

Singular value decomposition (SVD) of this matrix was calculated and divided into its input, output, and scalar components.

The covariance matrix SVD components were then applied to a Karhunen-Loève transform to create a synthetic SSH sample using the equation,

$$SSH_{syn} = SSH_{mean} + u\sigma n .$$

Where 'SSH_{mean}' is the vector for mean sea surface height, 'u' is the output control vector from the SVD of the covariance matrix, 'σ' is the scalar component matrix of the SVD of the covariance matrix, and 'n' is a vector that replaces the input vector calculated by the SVD of the covariance matrix with a set of random numbers generated by a random number generator.

To generate n, the 'randn' function in MATLAB was used with SSH_{mean} as its input. The randn function produced a vector of the of the same size as the input, with a Gaussian distribution of scalar values, where a value of 0 is equivalent to the mean while a value of 1 is equivalent to one standard deviation away from the mean. Positive and negative values indicate values greater and less than the mean, respectively.

By using this formula, synthetic SSH plots were created within the bounds of the variance of each month of SSH observed samples. Any changes in SSH were based on a Gaussian distribution centered on the average SSH for the particular month. The process was repeated for all months to produce synthetic SSH plots throughout the year.

In order to evaluate our results, for each individual month, we took the difference between the observed and synthetic SSH plots for monthly mean, variance, and covariance. Although we looked at individual SSH observation plots and individual SSH synthetic plots to get an idea of how close both those plots could be, given that some of the synthetic SSH plots could be wildly different from the observed plots, we made sure that as a whole, the variance, mean, and covariance of each observed month was closely related in each synthetic month. Since values within the synthetic SSH plots were based on a Guassian distribution of values, it was best to look at plots in terms of their monthly averages.

8. Results

Our data processing method allowed us to create synthetic SSH plots from the calculated monthly averages and variability of SSH in the Gulf of Mexico. A sample of observed plots compared to synthetic plots can be seen in Appendix E. Our intermediate steps, monthly plots of average SSH and SSH variance, can be seen in Appendices A and B, respectively. Our plots of the changes in the synthetic monthly mean and variance from the observed monthly mean and variance can be seen in appendices C and D, respectively.

In general, our plots of monthly mean SSH, both observed and synthetic, had their highest SSH values during the fall months of September and October

and their lowest values during spring in March and April. This seasonal variation was an expected consequence of solar heating of the upper ocean.

The synthetic and observed SSH monthly variance plots show areas of large variance in the same general area near the western edge of Cuba (the approximate area between 22-28°N and 84-90°W); the area where the LC bends and sheds warm water eddies. Areas of moderate SSH variance occur in the middle of the Gulf of Mexico, where shed eddies travel westward and dissipate. Their dissipation leads to less heat being transported into the western Gulf of Mexico, resulting in a decrease in variance at those grid nodes.

Looking at the difference between the observed and synthetic SSH mean, changes in mean SSH were on the order of plus or minus 5 cm with some anomalous areas up to plus or minus 10 cm. These anomalous regions were typically centered on the area of the eddy shedding region of the LC (near 25°N, 87°W).

The difference between the observed and synthetic SSH variance had little change except near the eddy shedding region of the LC. The area near the LC eddy shedding region had a difference in variance of 150-400 cm^2, although December and April had variance less than 150 cm^2 in this region. Away from the LC, the change in variance is considerably less and was in the range of 0-100 cm^2. The least change in variance occurred in the months of December and April while the greatest change occurred in the months of May and July.

9. Data Analysis

The synthetic SSH plots bear a good resemblance to the observed plots in that they have the same trends. Appendix E shows a sampling of observed plots compared to synthetic plots of SSH. The first page shows August samples while the second shows January samples. In the winter and spring months, SSH stays relatively low compared to SSH in the summer and fall months. However, areas showing considerably more variability, such as the eddy shedding region and region containing westward-travelling eddies, show significant differences between individual SSH plots. However, this should reflect the constantly changing influx of warm water into Gulf of Mexico based on the shedding of eddies from the LC. Given that eddies do not shed at regular intervals, one expects to see changes in the presence of new and old LC eddies. It can also reflect the change in the path of the LC. Increased SSH in the northeastern corner of the Gulf of Mexico can be a result of the LC bending to the north.

If one looks at large scale trends over the monthly average of SSH in both observed and synthetic datasets, the differences between both datasets are less pronounced. Appendix C shows the difference in observed and synthetic mean monthly SSH, while Appendix D shows the difference between observed and synthetic monthly SSH variances. Given that the differences between mean observed and mean synthetic SSH is considerably less than the difference between the SSH of individual observed and synthetic samples, on average, synthetic samples will be generated closer to the topography of the observed

samples. Given that the synthetic samples were generated using a Gaussian distribution, were more synthetic samples generated, their mean SSH and SSH variance should be closer and their difference plots should be near zero.

However, the difference plots in Appendices C and D show their greatest differences in the eddy shedding region. These differences are expected because of the non-regular frequency at which the LC changes direction and sheds eddies.

There may be some issues with the dataset relating to the resolution and land masking. It is very apparent that the land mask is rather approximate and does not take into account smaller land masses that exist in the Gulf of Mexico, for example, Florida and Cuba. Both of these land masses are larger than the resolution of the SSH data and thus should be included. On each plot, Mexico and the US Gulf Coast are part of the land mask, but Cuba and Central Florida are not included and SSH readings are located where land should exist. Thus, should a synthetic hurricane pass over these areas where land should be located, a hurricane intensity model will err since that area will be interpreted as ocean.

The land masking problem is part of the problem of needing more resolution. Without better resolution, parts of coastlines and islands will not be included and those areas will be interpreted as ocean, adding to error in hurricane intensity models. In addition, more resolution will allow for a more accurate account of the amount of heat content in the upper ocean mixed layer; the heat needed for hurricane formation and development. A better measure of

heat content in the upper ocean will allow for better accuracy in determining hurricane intensity.

10. Discussion

The model was able to generate synthetic plots of SSH that can provide another step in improving hurricane intensity modeling. Now with monthly averages of SSH along with the variance and covariance of SSH in the Gulf of Mexico, more specific hurricane intensity models can be made for the month instead of the season. With monthly synthetic estimates of SSH, better estimates of hurricane intensity can be made and thus one can discover the risk associate with storms in a particular month instead of an entire season.

However, the generation of these synthetic plots only takes into account SSH observations from the last 15 years and may not be representative of average SSH readings over the longer term. Since satellite laser altimetry measurement has only existed for the past couple decades, SSH trends for the past century or beyond can only be speculated upon. One way possible way to extrapolate from past values is to use sea surface temperature (SST). SST measurements have been around since the age of sailing vessels, but more complete SST data started in the 1970 with the advent of infrared satellites (Emery, 2001). Using SST data, one could try to estimate heat content in the upper ocean and SSH, but SST does not give a clear picture of the temperature structure in the upper ocean since infrared satellites can only penetrate 10 μm

beyond the surface of the ocean while ships and buoys generally make measurements between 0.5m-5m (Emery, 2001). Argo floats have only been placed in the last few years, but will give us a better picture of upper ocean temperature structure (Roemmich, 2000). Thus, a model could be made to estimate past SSH with SST, but there will still be uncertainty about the temperature profile, which will generate uncertainty and inaccuracy in estimating past SSH values.

Not only can we only speculate about the specific SSH values in past decades, but there is also some uncertainty in modeling SSH in the future. Global climate change can have implications for SSH readings in the future. Given that global climate change has the potential to significantly heat the oceans, additional oceanic heat content and thermosteric sea level rise will also increase SSH values (Willis, 2004). In order for the synthetic SSH model to be more accurate in the future, it must take into account climate change.

In the short term, the model described here is a starting point in quantifying monthly fluctuations of SSH in the Gulf of Mexico. However, with continued SSH observation from laser altimetry satellite missions, we can hope to understand more of the SSH variability throughout the year. In addition, we can also understand more about long term changes in SSH. With better estimations of past and future SSH, the synthetic SSH model can be improved and will provide a better input for hurricane intensity models. Improved hurricane models will lead to improved risk assessments for coastal communities throughout the world and will help reduce the economic problems associated with

large storms by giving governments, companies, and individuals proper preparation.

References

Cione, J. J., & Uhlhorn, E.W. 2003, Sea Surface Temperature Variability in Hurricanes: Implications with Respect to Intensity Change, *Monthly Weather Review*, v. 131, p. 1783-1796.

Emanuel, K.A. 1999, Thermodynamic Control of Hurricane Intensity, *Nature*, v. 401, p. 665-669.

Emanuel, K.A. 2003, Tropical Cyclones, *Annual Review of Earth and Planetary Sciences*, v. 31, p. 75-104.

Emanuel, K.A. 2004, Tropical Cyclone Energetics and Structure, *Atmospheric Turbulence and Mesoscale Meteorology*, Cambridge University Press, 165-192

Emanuel, K.A., Ravela, S., Vivant, E., & Risi, C. 2006, A Statistical Deterministic Approach to Hurricane Risk Assessment, *Bulletin of the American Meteorological Society*, v. 87, p. 299-314.

Emery, W.J., Castro, S., Wick, G.A., Schluessel, P., & Donlon, C. 2001, Estimating Sea Surface Temperature from Infrared Satellite and In Situ Temperature Data, *Bulletin of the American Meteorological Society*, v. 82, p. 2773-2785.

Fu, L-L., Christensen, E., Yamarone, C. Jr., Lefebvre, M., Menard, Y., Dorrer, M., & Escudier, P. 1994, TOPEX/POSEIDON mission overview, *Journal of Geophysical Research*, v. 99, p. 24369-24382.

Hurlbut, H.E., & Thompson, D J. 1980, A Numerical Study of Loop Current Intrusions and Eddy Shedding, *Journal of Physical Oceanography*, v. 10, p1611-1651.

Leipper, D, & Volgenau, D. 1972, Hurricane Heat Potential of the Gulf of Mexico, *Journal of Physical Oceanography*, v. 2, p. 218-224.

Levitus, S. 1982, Annual Cycle of Temperature and Heat Storage in the World Ocean, *Journal of Physical Oceanography*, v. 14, p.727-746.

Lin, I-I, & Wu, C-C. 2005, The Interaction of Supertyphoon Maemi (2003) with a Warm Ocean Eddy, *Monthly Weather Review*, v. 133, p. 2635–2649.

Marks, F. D. 1985, Evolution of the Structure of Precipitation in Hurricane Allen (1980), *Monthly Weather Review*, v. 113, p.909-930.

Oey, L., & Lee, H. 2003, Effects of Winds and Caribbean Eddies on the Frequency of Loop Current Eddy Shedding: A Numerical Model Study, *Journal of Geophysical Research*, v. 108, p. 22.1-22.25

Risk Management Solutions. (2005, September 9). Great New Orleans Flood to Contribute Additional $15-$25 Billion in Private Sector Insured Losses for Hurricane Katrina, Bringing Estimated Insured Losses to $40-$60 Billion. [WWW Document]. URL http://rms.com/newspress/pr_090205_hukatrina_insured_update.asp (visited 2007, November 19).

Roemmich, D., & Owens, W.B. 2000, The Argo Project: Global Ocean Observations for Understanding and Prediction of Climate Variability, *Oceanography*, v. 13, p. 45-50.

Smith, W.H.F., & Sandwell, D.T. 1997. Global Sea Floor Topography from Satellite Altimetry and Ship Depth Soundings, *Science*, v. 277, p. 1956-1962.

USA Today. (2005, September 9). Katrina damage estimate hits $125B. [WWW Document]. URL http://www.usatoday.com/money/economy/2005-09-09-katrina-damage_x.htm (visited 2007, November 19)

Willis, J. K. 2004, Interannual Variability in Upper Ocean Heat Content, Temperature, and Thermosteric Expansion on Global Scales, *Journal of Geophysical Research*, v. 109, C12036.

Willoughby, H. E. 1999, Hurricane Heat Engines, *Nature*, v. 401, p. 649-650.

Zavala-Hidalgo, J., Morey, S.L., O'Brien, J.J., & Zamudio, L. 2005, On Loop Current Shedding Variability, *Atmosfera*, v. 19, p. 41-48.

Appendix A – Observed Monthly SSH Averages

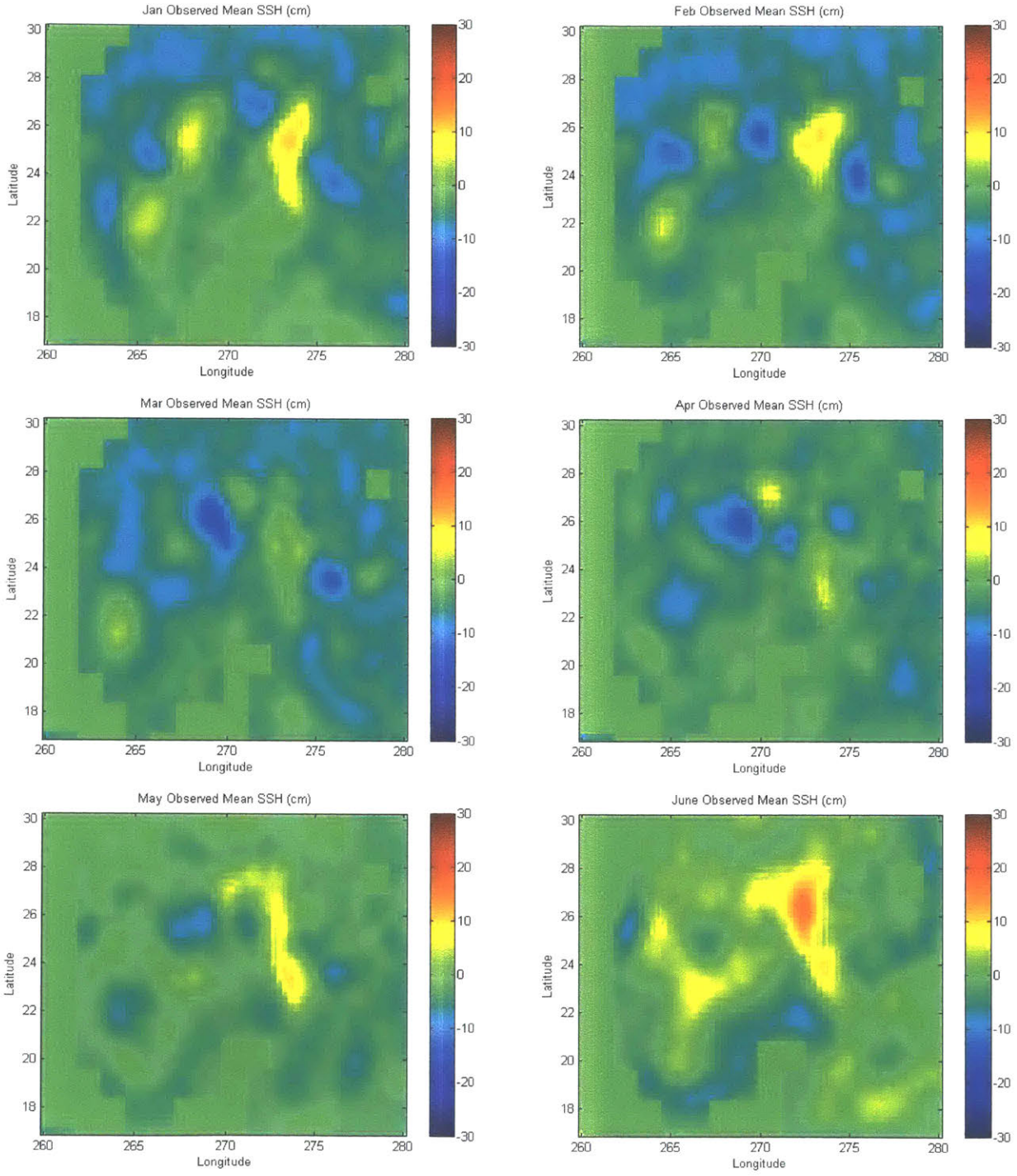

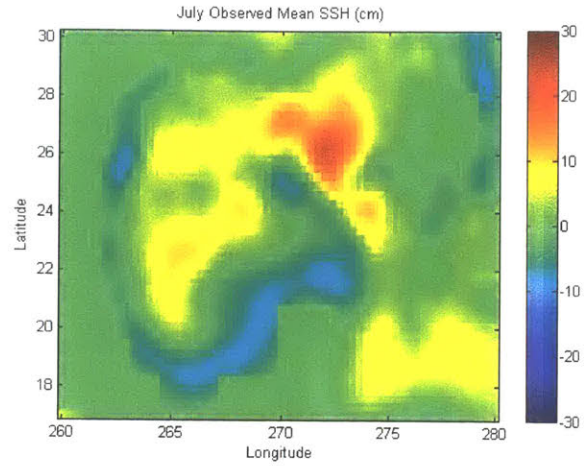
July Observed Mean SSH (cm)
Latitude
Longitude
30
28
26
24
22
20
18
260
265
270
275
280
30
20
10
0
-10
-20
-30

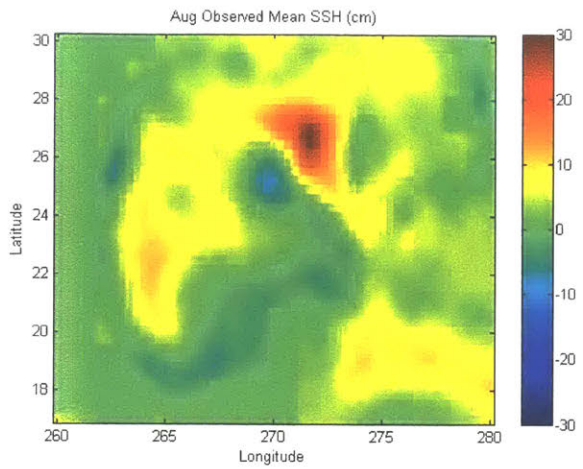
Aug Observed Mean SSH (cm)
Latitude
Longitude
30
28
26
24
22
20
18
260
265
270
275
280
30
20
10
0
-10
-20
-30

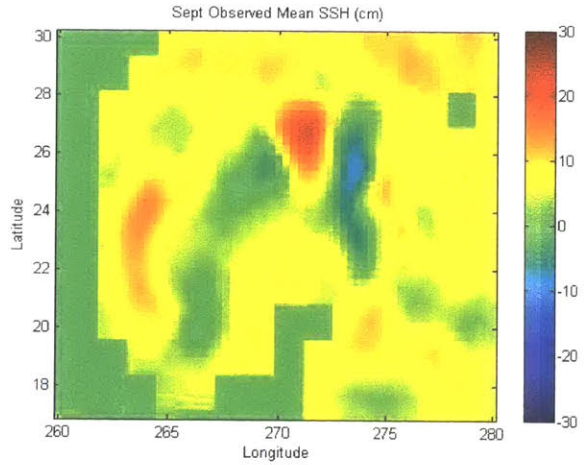
Sept Observed Mean SSH (cm)
Latitude
Longitude
30
28
26
24
22
20
18
260
265
270
275
280
30
20
10
0
-10
-20
-30

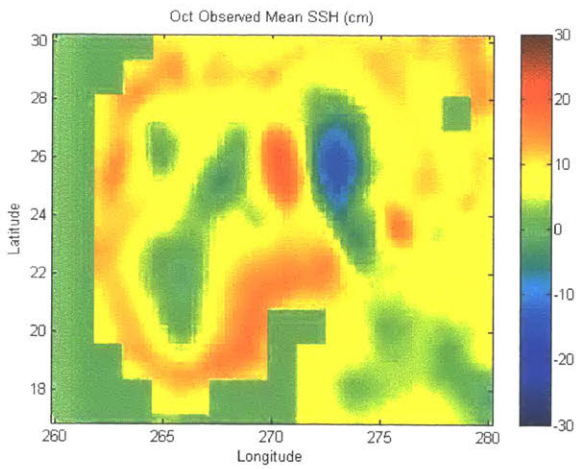
Oct Observed Mean SSH (cm)
Latitude
Longitude
30
28
26
24
22
20
18
260
265
270
275
280
30
20
10
0
-10
-20
-30

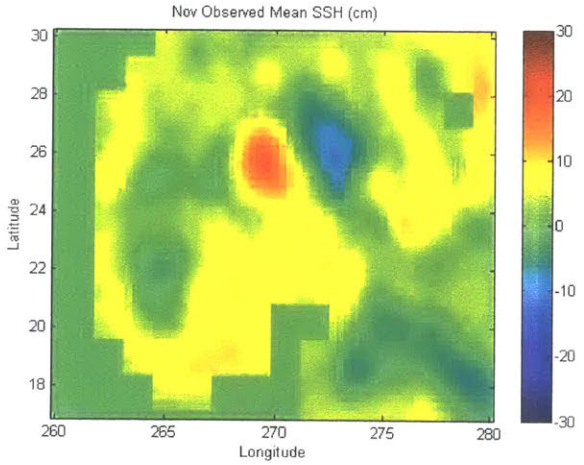
Nov Observed Mean SSH (cm)
Latitude
Longitude
30
28
26
24
22
20
18
260
265
270
275
280
30
20
10
0
-10
-20
-30

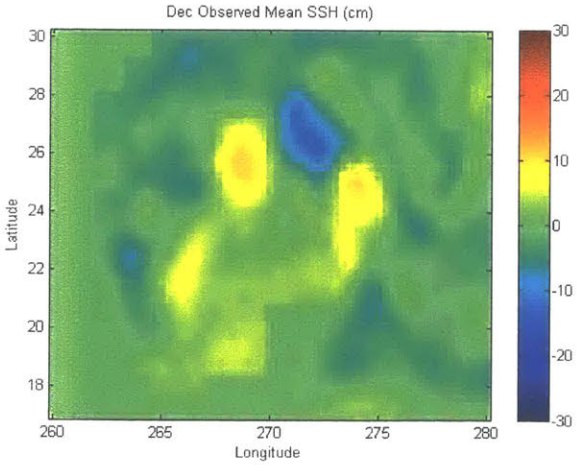
Dec Observed Mean SSH (cm)
Latitude
Longitude
30
28
26
24
22
20
18
260
265
270
275
280
30
20
10
0
-10
-20
-30

Appendix B – Observed Monthly SSH Variance

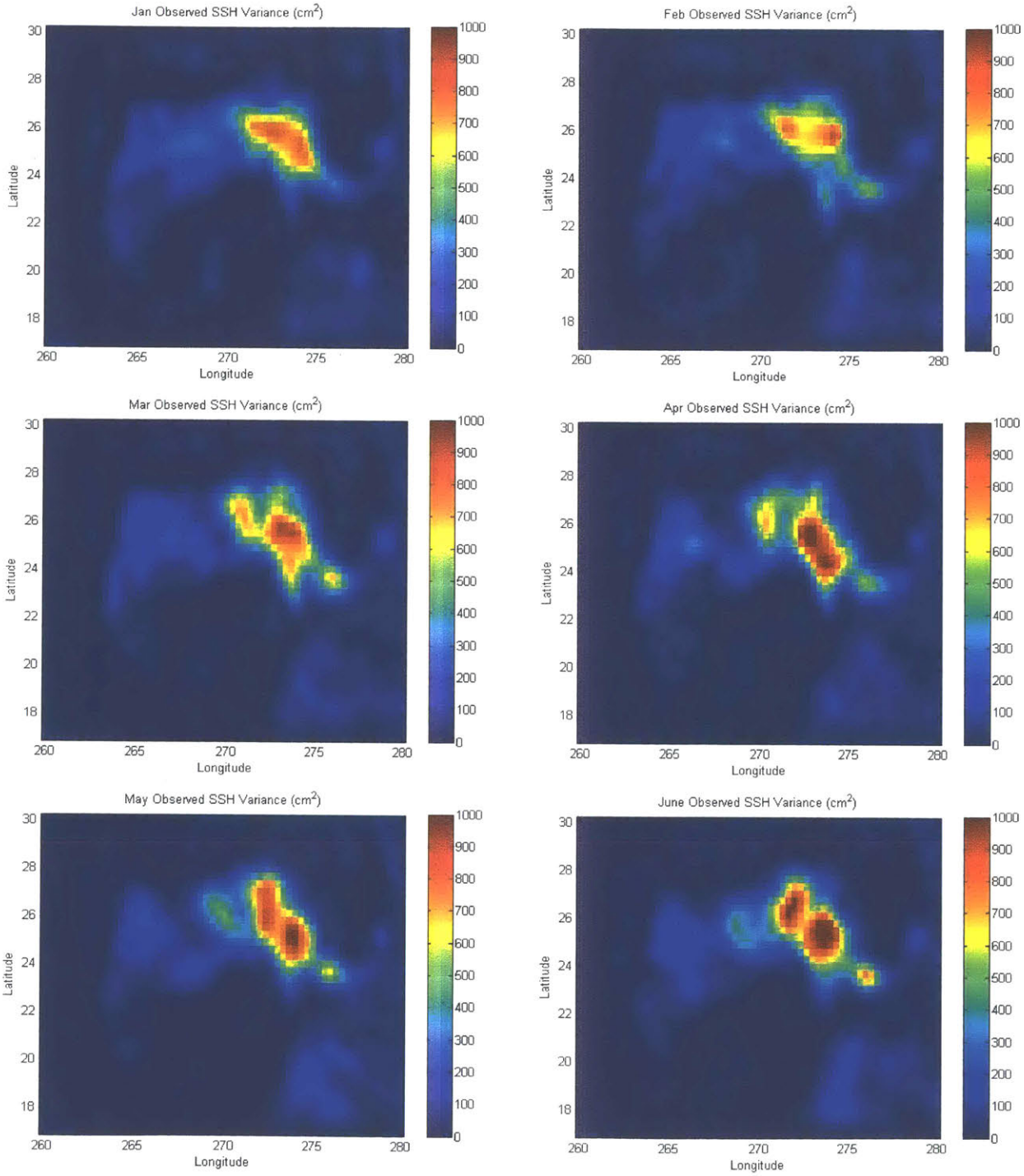

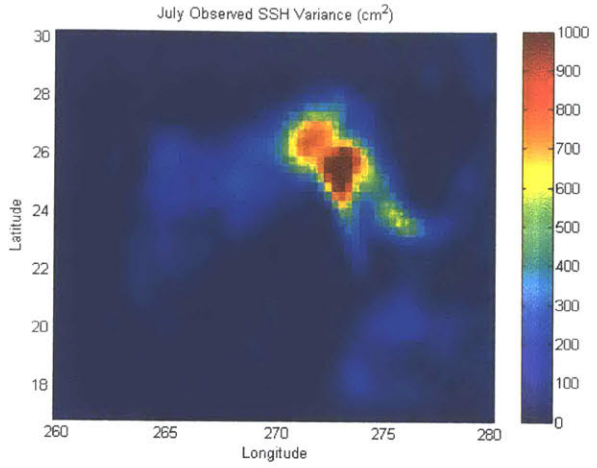
July Observed SSH Variance (cm^2)
Latitude
Longitude
30
28
26
24
22
20
18
260
265
270
275
280
1000
900
800
700
600
500
400
300
200
100
0

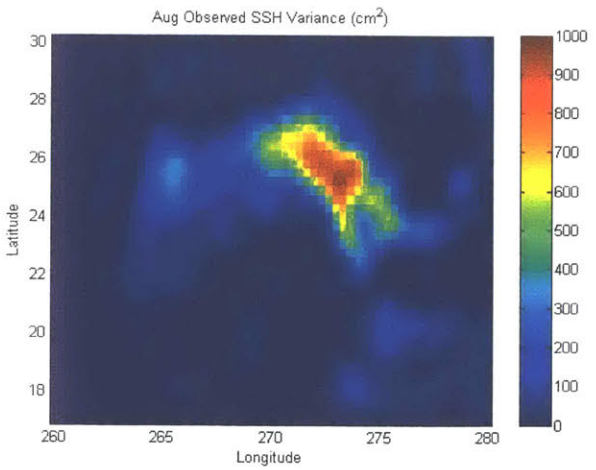
Aug Observed SSH Variance (cm^2)
Latitude
Longitude
30
28
26
24
22
20
18
260
265
270
275
280
1000
900
800
700
600
500
400
300
200
100
0

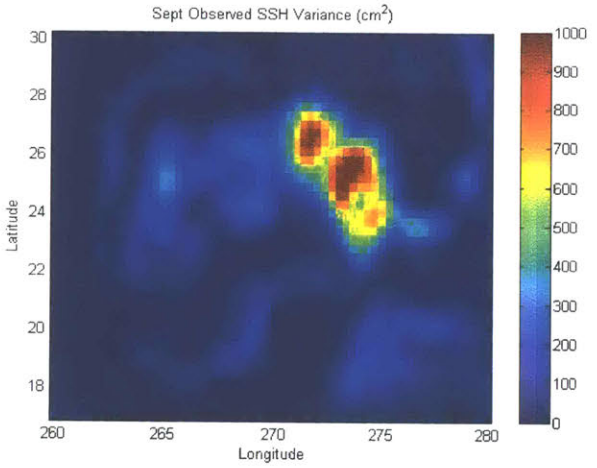
Sept Observed SSH Variance (cm^2)
Latitude
Longitude
30
28
26
24
22
20
18
260
265
270
275
280
1000
900
800
700
600
500
400
300
200
100
0

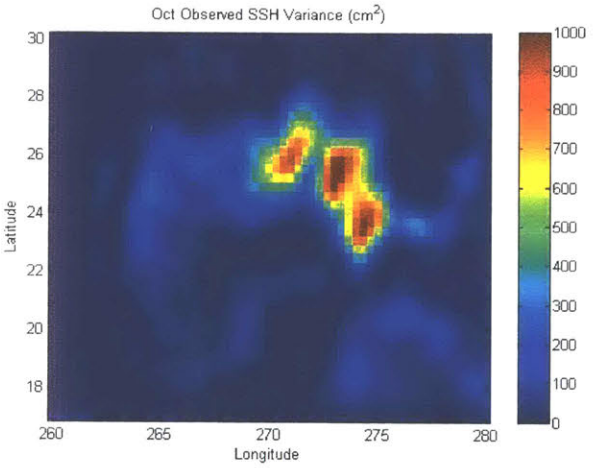
Oct Observed SSH Variance (cm^2)
Latitude
Longitude
30
28
26
24
22
20
18
260
265
270
275
280
1000
900
800
700
600
500
400
300
200
100
0

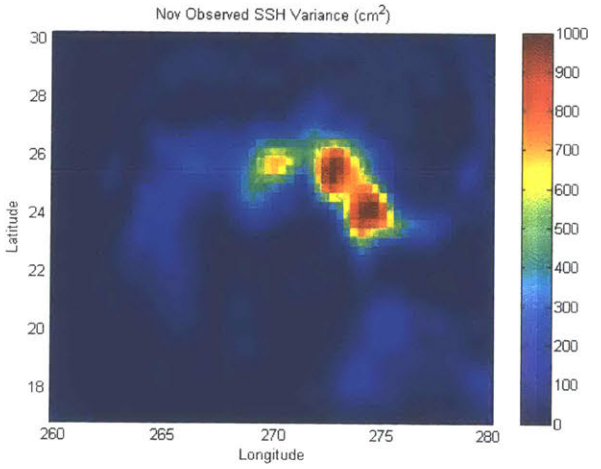
Nov Observed SSH Variance (cm^2)
Latitude
Longitude
30
28
26
24
22
20
18
260
265
270
275
280
1000
900
800
700
600
500
400
300
200
100
0

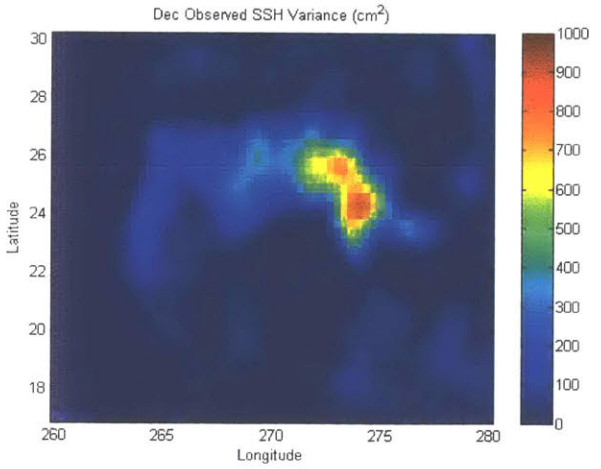
Dec Observed SSH Variance (cm^2)
Latitude
Longitude
30
28
26
24
22
20
18
260
265
270
275
280
1000
900
800
700
600
500
400
300
200
100
0

Appendix C – Difference Plots Between Observed and Synthetic Average SSH Data

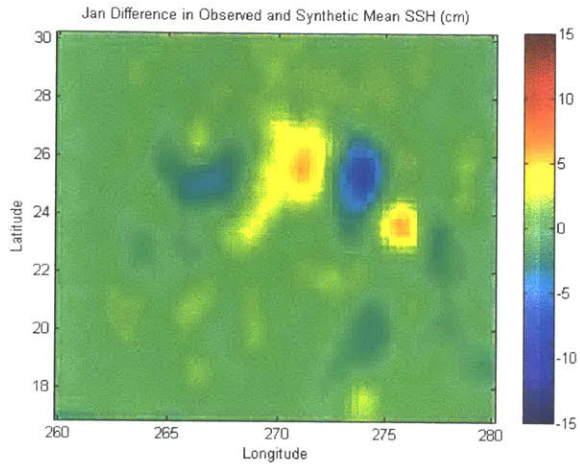

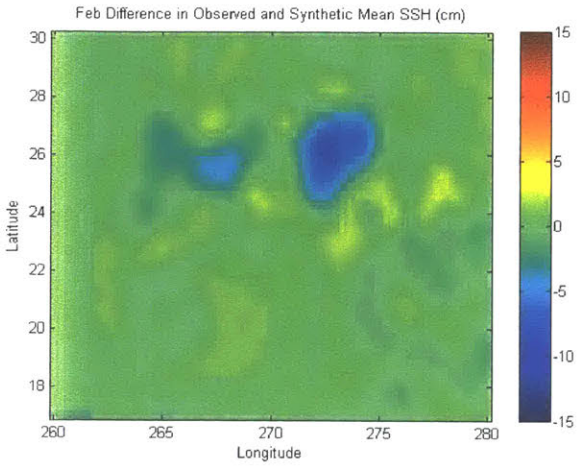

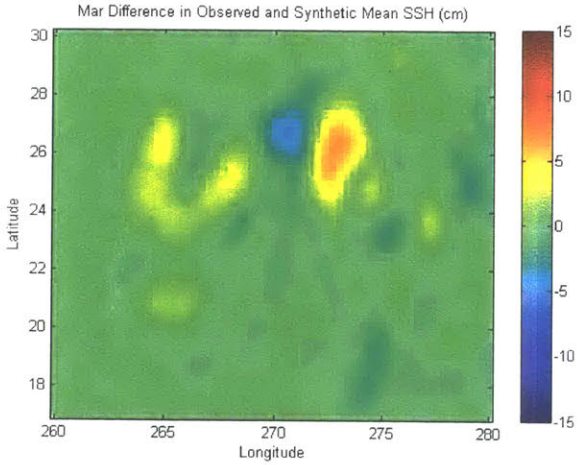

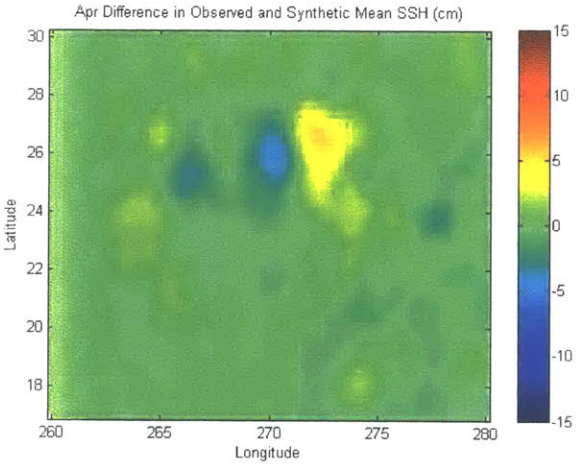

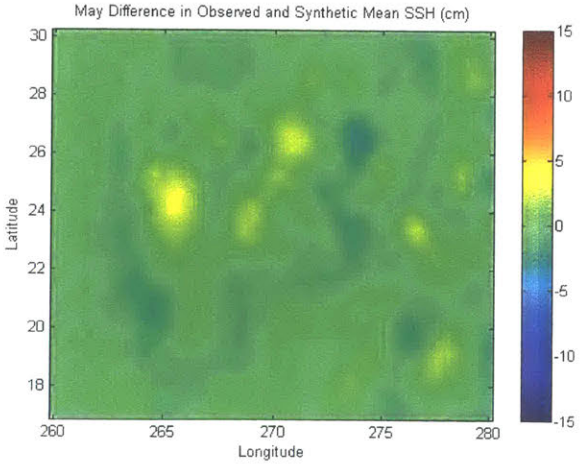

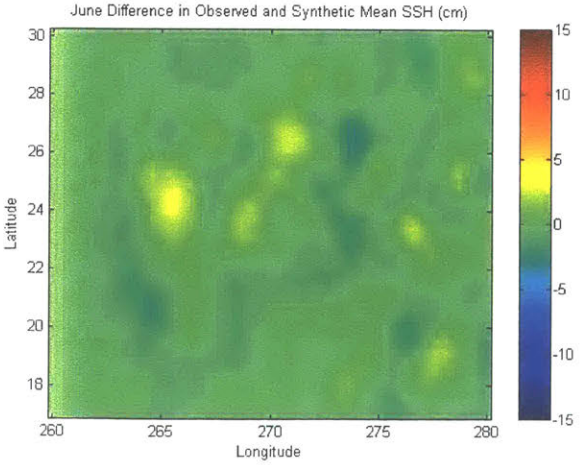

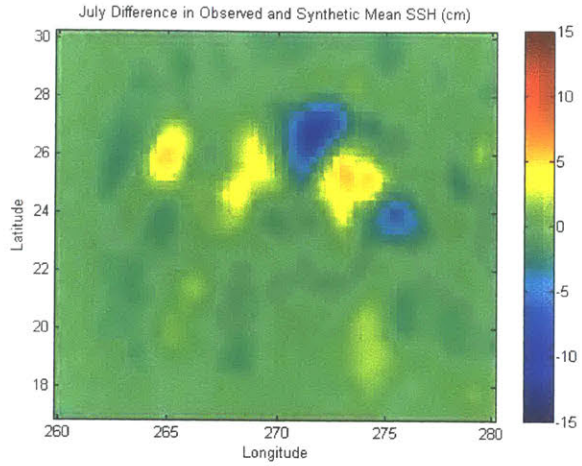
July Difference in Observed and Synthetic Mean SSH (cm)
Latitude
Longitude
30
28
26
24
22
20
18
260
265
270
275
280
15
10
5
0
-5
-10
-15

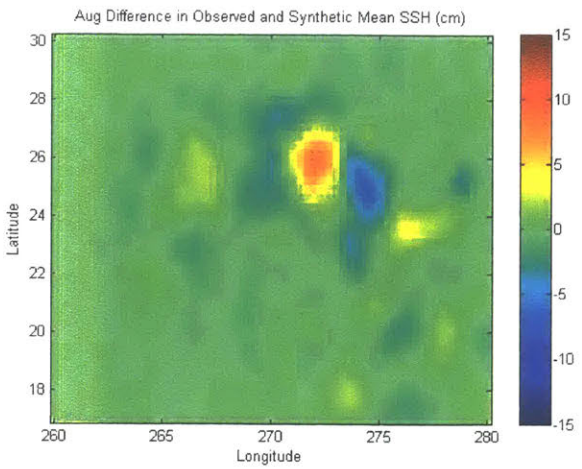
Aug Difference in Observed and Synthetic Mean SSH (cm)
Latitude
Longitude
30
28
26
24
22
20
18
260
265
270
275
280
15
10
5
0
-5
-10
-15

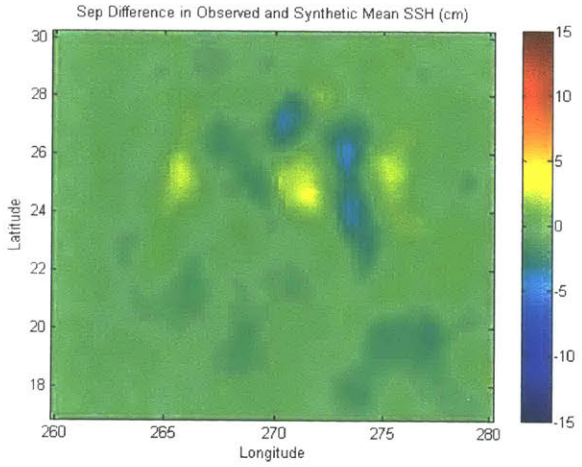
Sep Difference in Observed and Synthetic Mean SSH (cm)
Latitude
Longitude
30
28
26
24
22
20
18
260
265
270
275
280
15
10
5
0
-5
-10
-15

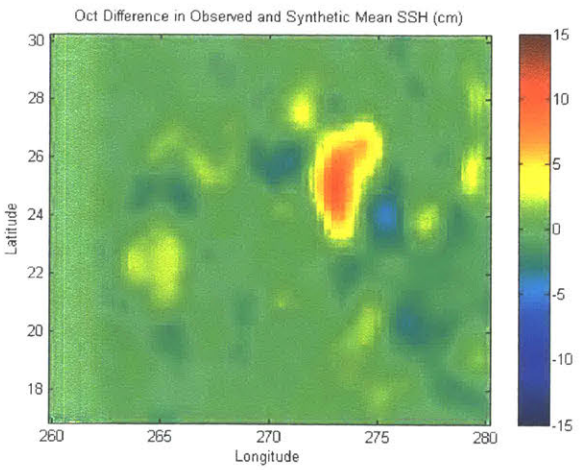
Oct Difference in Observed and Synthetic Mean SSH (cm)
Latitude
Longitude
30
28
26
24
22
20
18
260
265
270
275
280
15
10
5
0
-5
-10
-15

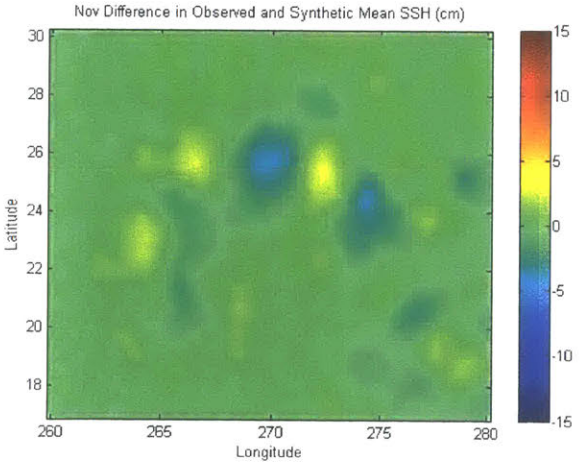
Nov Difference in Observed and Synthetic Mean SSH (cm)
Latitude
Longitude
30
28
26
24
22
20
18
260
265
270
275
280
15
10
5
0
-5
-10
-15

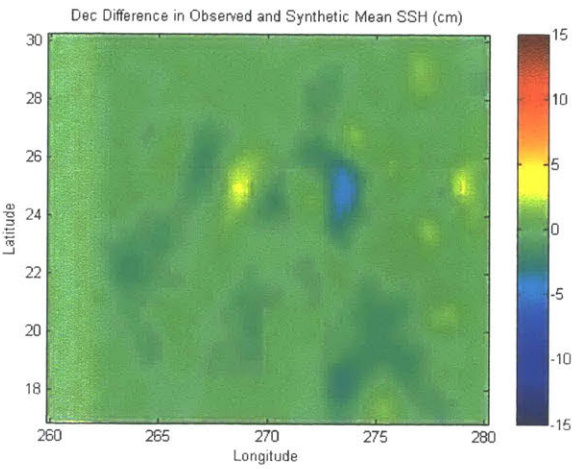
Dec Difference in Observed and Synthetic Mean SSH (cm)
Latitude
Longitude
30
28
26
24
22
20
18
260
265
270
275
280
15
10
5
0
-5
-10
-15

Appendix D – Difference Plots Between Observed and Synthetic SSH Variance Data

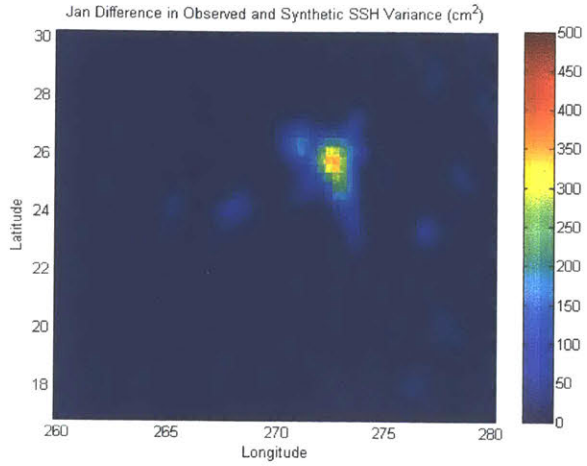

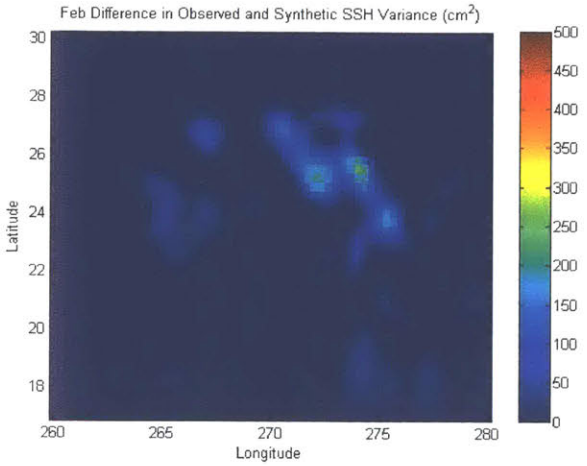

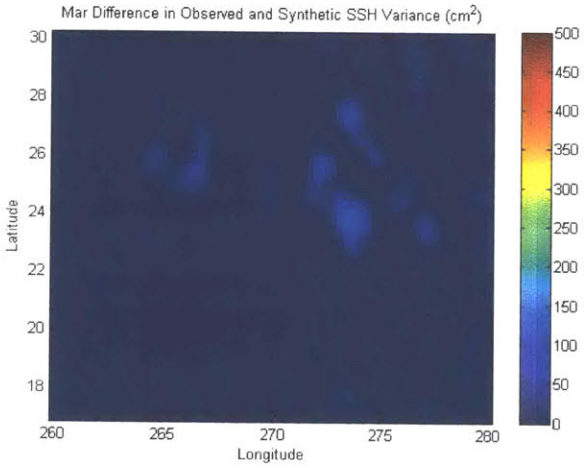

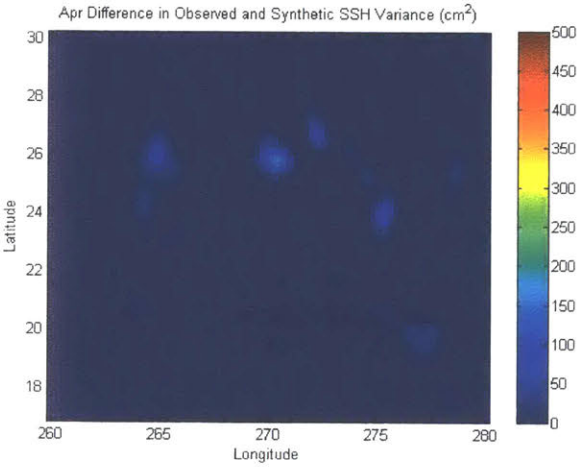

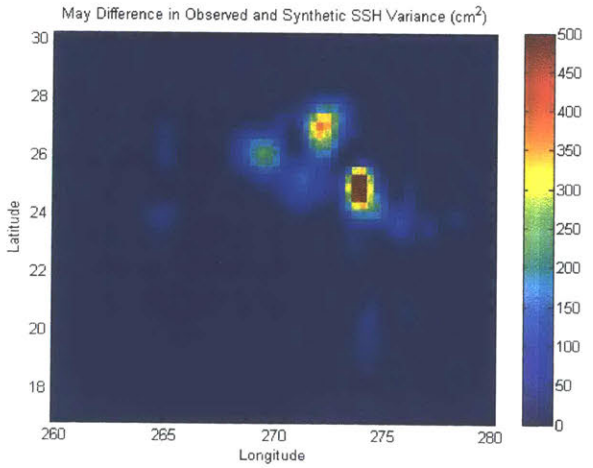

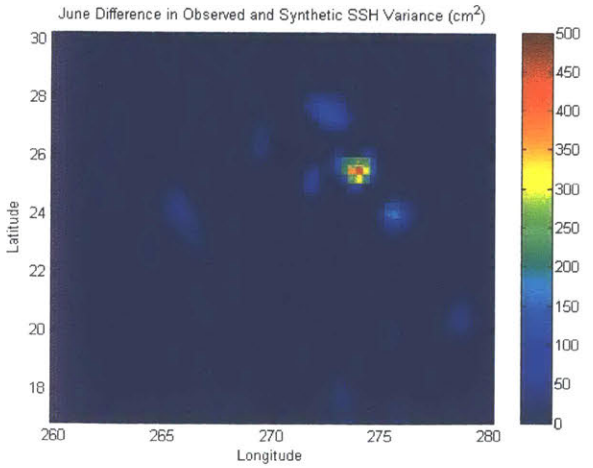

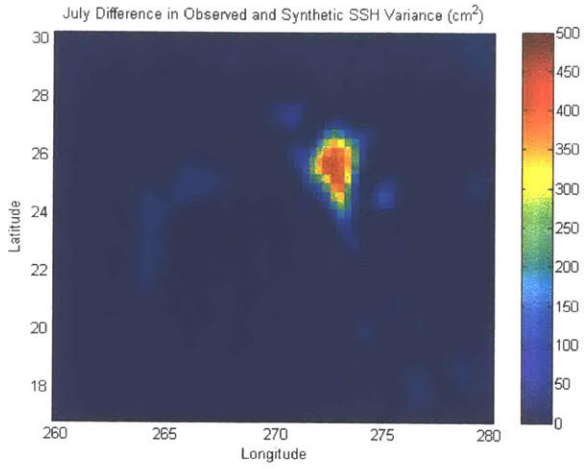
July Difference in Observed and Synthetic SSH Variance (cm^2)
Latitude
Longitude
30
28
26
24
22
20
18
260
265
270
275
280
500
450
400
350
300
250
200
150
100
50
0

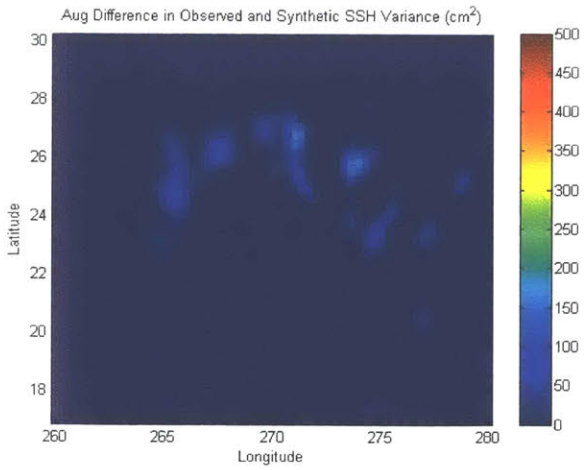
Aug Difference in Observed and Synthetic SSH Variance (cm^2)
Latitude
Longitude
30
28
26
24
22
20
18
260
265
270
275
280
500
450
400
350
300
250
200
150
100
50
0

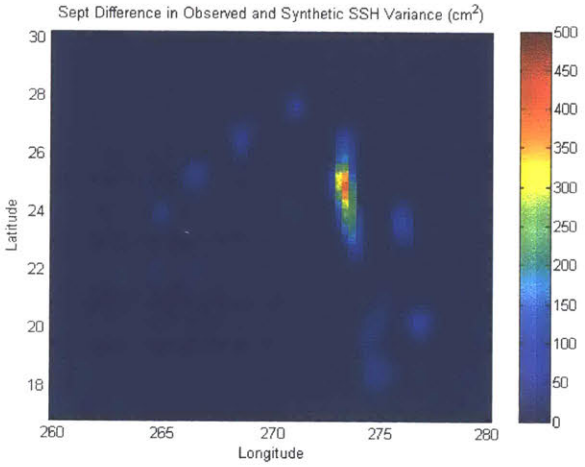
Sept Difference in Observed and Synthetic SSH Variance (cm^2)
Latitude
Longitude
30
28
26
24
22
20
18
260
265
270
275
280
500
450
400
350
300
250
200
150
100
50
0

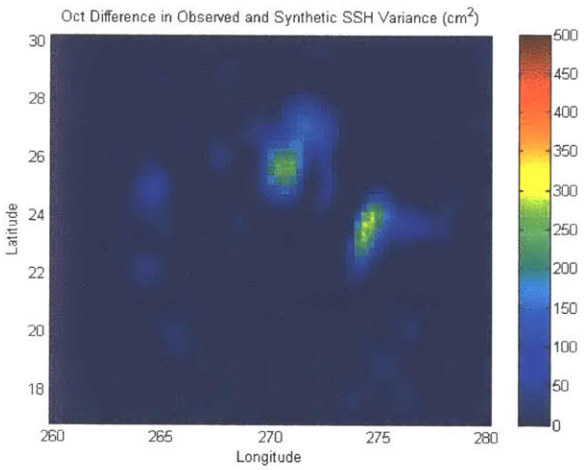
Oct Difference in Observed and Synthetic SSH Variance (cm^2)
Latitude
Longitude
30
28
26
24
22
20
18
260
265
270
275
280
500
450
400
350
300
250
200
150
100
50
0

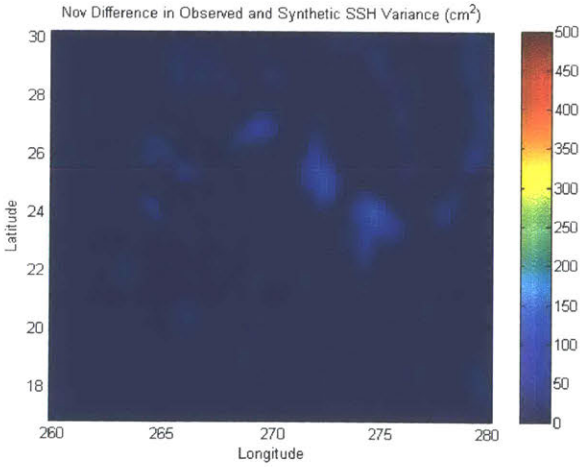
Nov Difference in Observed and Synthetic SSH Variance (cm^2)
Latitude
Longitude
30
28
26
24
22
20
18
260
265
270
275
280
500
450
400
350
300
250
200
150
100
50
0

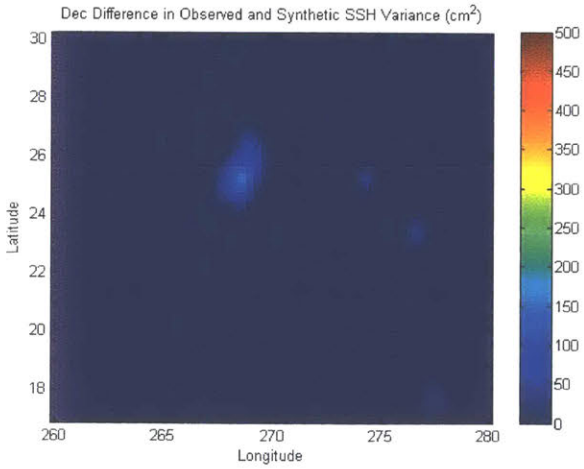
Dec Difference in Observed and Synthetic SSH Variance (cm^2)
Latitude
Longitude
30
28
26
24
22
20
18
260
265
270
275
280
500
450
400
350
300
250
200
150
100
50
0

Appendix E – Observed and Synthetic SSH Samples

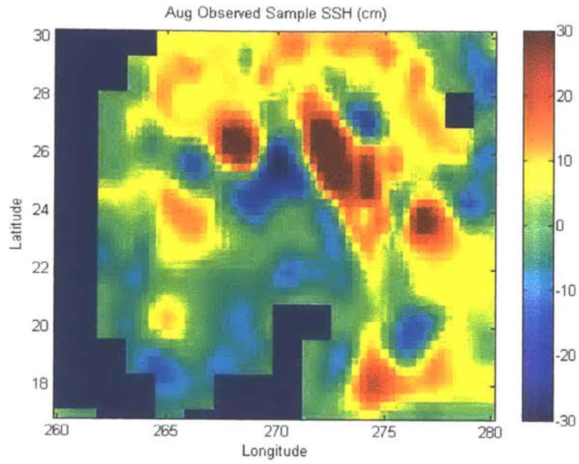

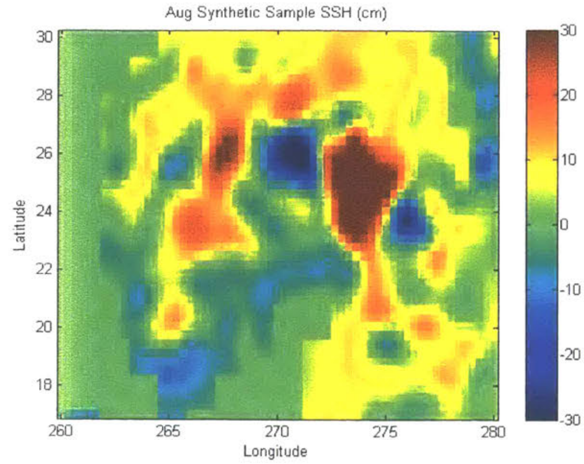

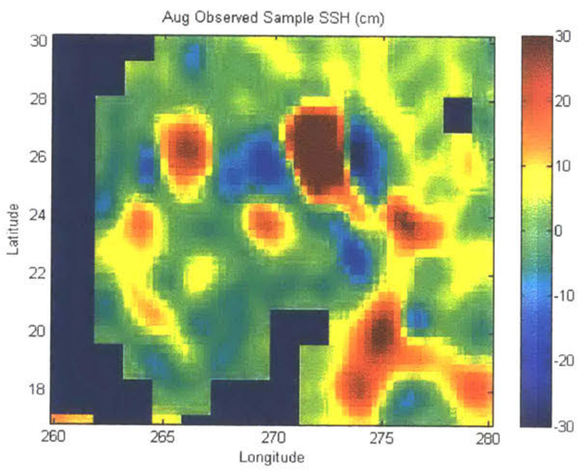

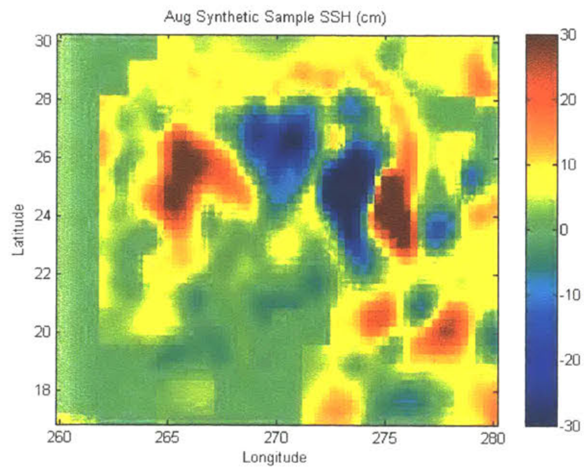

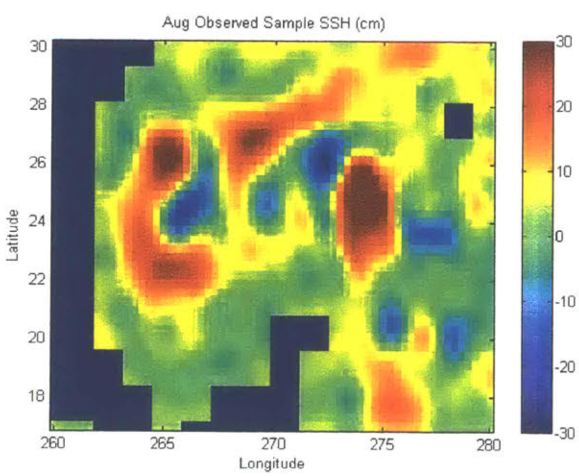

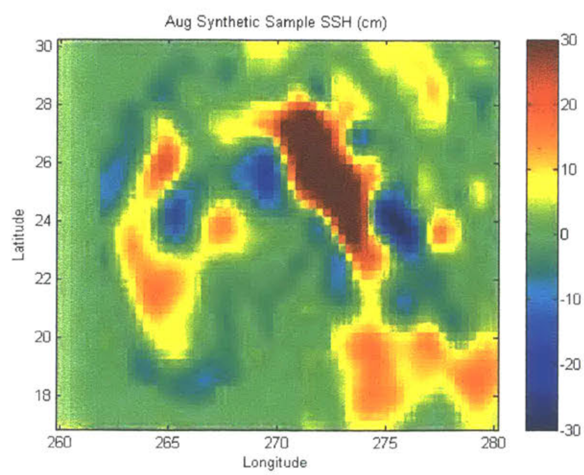

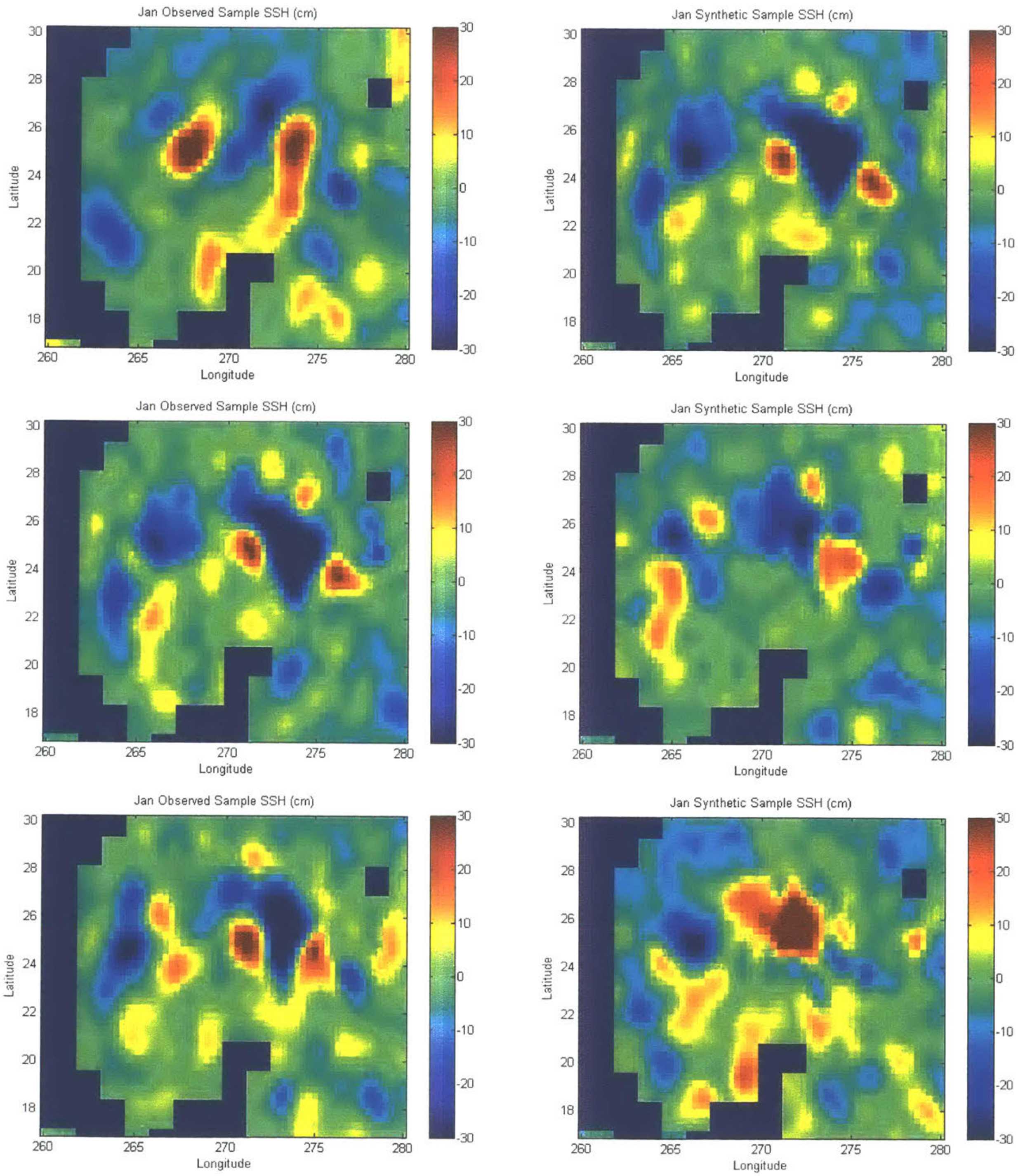
Jan Observed Sample SSH (cm)
Jan Synthetic Sample SSH (cm)
Jan Observed Sample SSH (cm)
Jan Synthetic Sample SSH (cm)
Jan Observed Sample SSH (cm)
Jan Synthetic Sample SSH (cm)
Latitude
Longitude